ICOSSAR 2005, G. Augusti, G.I. Schuëller, M. Ciampoli (eds)
 ISBN 90 5966 040 4

On the use of proper orthogonal decomposition to describe inflow turbulence and wind turbine loads

K. Saranyasoontorn & L. Manuel
Department of Civil Engineering, University of Texas at Austin, TX, USA

Keywords: Proper Orthogonal Decomposition, inflow turbulence, wind turbine

ABSTRACT: We discuss an application of Proper Orthogonal Decomposition (POD) to characterize the inflow turbulence random field experienced by a wind turbine. A methodology is proposed that employs low-dimensional POD models of the turbulence field to predict the wind turbine load statistics for the design purposes. The efficiency of the proposed strategy is assessed by evaluating rates of convergence of load statistics derived based on different numbers of inflow POD modes. Influence on convergence due to different spatial and temporal sampling resolutions of the inflow data is also investigated. Results suggest that the appropriate number of POD modes needed to accurately describe wind turbine blade and tower loads depends primarily on the dynamic characteristics of the turbine loads under consideration as well as on the rotational sampling of the inflow turbulence. In general, a small number of inflow POD modes can faithfully account for the low-frequency energy in the turbine load measures studied. At higher frequencies, where the inflow turbulence field exhibits weak coherence at spatial separations on the order of rotor dimensions, a larger number of modes may be required. Based on this study limited to a single two-bladed 600 kW wind turbine, results from several spatial and temporal samplings of the inflow turbulence show that data from spatial grids with dimensions on the order of one-third the rotor diameter and sampling frequencies of 2.5-5 Hz or higher can yield adequate representations of important POD modes useful for establishing accurate turbine loads. This was verified by comparing loads resulting from such efficient POD representations of inflow fields with those from sampled data on very fine grids and at high sampling rates.

1 INTRODUCTION

Proper Orthogonal Decomposition (POD) is a powerful numerical technique that can be used to efficiently identify preferred patterns/modes of spatio-temporal random fields and then employ low-dimensional representations of such fields using the derived modes. A limited number of POD modes is often sufficient to account for most of the energy of the entire random field. Historically, POD techniques were developed independently during the same period of time by several investigators including Kosambi (1943), Karhunen (1946), and Loève (1948). Mathematically, the POD procedure involves a search for deterministic orthogonal basis functions for representations of complex spatio-temporal fields and is optimal in the sense that it converges (in L^2-norm) faster on average than any other linear decomposition technique. Because of this optimality, the method has been employed in many science and engineering applications such as turbulent fluid flows (Lumley, 1970; Holmes et al, 1997), wind engineering (Carassale & Solari, 2000; Chen & Kareem, 2003), turbulence and atmospheric stability (Spitler et al, 2004), etc. Recently, Saranyasoontorn & Manuel (2005) demonstrated the usefulness of the POD procedure in describing dominant features of the along-wind turbulence random field experienced by a typical wind turbine. They showed that a small number of inflow POD modes was sufficient for use in deriving wind turbine load statistics. In the present study, we extend that previous study and seek to examine in greater detail the efficiency of a POD in wind turbine load analysis. The varying turbine dynamic modes for the different turbine load measures (for the blade and the tower, for example) and the rotational sampling of the inflow turbulence are considered in discussions of the efficiency of low-dimensional POD representations for these loads.

Having illustrated that low-dimensional representations are possible using POD and that such representations can help establish accurate loads for design, an obvious next question is how should one efficiently collect the required data from which the POD modes can be derived. Clearly, the few important POD modes that are typically needed must be based on sampling of multiple inflow turbulence streams. Hence, another focus of the present study is on the selection from among several different spatial distributions of sensors (anemometers, here) and associated temporal sampling that is adequate to yield the POD modes and retain the critical dynamic features that influence each turbine load of interest. Efficient spatial distribution of sensors and associated sampling in time of turbulence when derived in this manner so as to allow accurate energy representation of the field can lead to economy in any planned experimental campaign that is focused on collecting spatio-temporal inflow data that directly influences loads.

We begin with a brief review of the theoretical framework for POD analysis. The accuracy of a POD-based reduced-order inflow representation to describe an inflow turbulence field and wind turbine load statistics is discussed next. Finally, we discuss selection from among alternative spatial and temporal sampling schemes for inflow turbulence sensors.

2 PROPER ORTHOGONAL DECOMPOSITION

In the following, we present the key concepts upon which POD is based. Several different formulations are available in the literature (see, for example, Holmes et al, 1996).

In one form of Proper Orthogonal Decomposition, called in some places Covariance Proper Transformation (CPT), assume that one is given N weakly stationary zero-mean correlated random processes, $\boldsymbol{V}(t) = \{V_1(t), V_2(t), \ldots V_N(t)\}^T$, and a corresponding $N \times N$ covariance matrix, $\mathbf{C_V}$. It is possible to diagonalize $\mathbf{C_V}$ so as to obtain the (diagonal) matrix, $\boldsymbol{\Lambda}$.

$$\boldsymbol{\Phi}^T \cdot \mathbf{C_V} \cdot \boldsymbol{\Phi} = \boldsymbol{\Lambda}; \quad \mathbf{C_V} \cdot \boldsymbol{\Phi} = \boldsymbol{\Phi} \cdot \boldsymbol{\Lambda}; \quad \boldsymbol{\Lambda} = \mathrm{diag}\{\lambda_1, \lambda_2, \ldots \lambda_N\} \tag{1}$$

The eigenvectors, $\boldsymbol{\Phi} = \{\boldsymbol{\phi}_1, \boldsymbol{\phi}_2, \ldots \boldsymbol{\phi}_N\}$ of $\mathbf{C_V}$ describe basis functions in a principal space. It is now possible to rewrite the original N correlated processes, $\boldsymbol{V}$(t), in terms of N uncorrelated *scalar* sub-processes, $\boldsymbol{a}(t) = \{a_1(t), a_2(t), \ldots a_N(t)\}^T$ such that

$$\boldsymbol{V}(t) = \boldsymbol{\Phi} \cdot \boldsymbol{a}(t) = \sum_{j=1}^{N} \boldsymbol{\phi}_j a_j(t) \tag{2}$$

where the uncorrelated scalar sub-processes can be derived by employing the orthogonality property,

$$\boldsymbol{a}(t) = \boldsymbol{\Phi}^T \cdot \boldsymbol{V}(t) \tag{3}$$

The covariance matrix for $\boldsymbol{a}(t)$, namely $\mathbf{C_a}$, is equal to the diagonal matrix, $\boldsymbol{\Lambda}$, and an energy measure associated with each $a_j(t)$ can be defined in terms of its variance, λ_j. The original random processes are conveniently decomposed into N uncorrelated random processes. If the eigenvalues, λ_j, are sorted in decreasing order, a reduced-order representation, $\hat{V}(t)$, is obtained by only retaining the first M covariance-based POD modes as follows:

$$\hat{\boldsymbol{V}}(t) = \sum_{j=1}^{M} \boldsymbol{\phi}_j a_j(t), \text{ where } M < N \tag{4}$$

Note that in the description above, $\boldsymbol{V}(t)$, can represent scalar turbulence random processes at N different locations defined for a single direction, but it could also represent all three components of turbulence at various locations.

3 NUMERICAL EXAMPLES

In this section, we assess the efficiency of reduced-order models of the inflow turbulence random field based on POD by studying the energy in such truncated inflow fields as well as turbine load statistics derived from them. This is done by comparisons with a full-field representation that involves no decomposition.

In the numerical studies, 10 ten-minute simulations of an inflow turbulence random field were generated with a sampling frequency of 20 Hz over the rotor plane of the National Wind Technology Center's Advanced Research Turbine (ART). This turbine (Fig. 1(a)) is a 600-kW, upwind, two-bladed, teetered-hub turbine with a hub height of 36.6 m, a rotor diameter of about 42 m, and a constant rotor speed of 42 rpm. The computer program, SNwind (Buhl, 2003) was used to carry out inflow field simulations. The Kaimal spectral model and the exponential coherence model recommended in the IEC guidelines (IEC, 1998) for wind turbine design were employed for the simulations. A 10×10 square grid discretization of the rotor plane was used as shown in Fig. 1(b). This implies that a total of 100 inflow POD modes can be defined to represent this field, where our focus is on the along-wind (u) component of the turbulence. (We showed in Saranyasoontorn & Manuel (2005) that the across-wind (v) and vertical (w) turbulence components have relatively far less influence on turbine loads.)

(a)

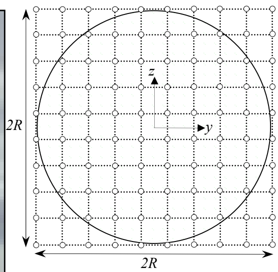

(b)

Figure 1. (a) ART machine;
(b) Spatial grid for simulations of turbulence on the 42 m × 42 m rotor plane.

© 2005 Millpress, Rotterdam, ISBN 90 5966 040 4

3.1 *POD representations of the inflow field*

Empirical orthogonal modes of the simulated inflow turbulence field were derived from the 100×100 sample covariance matrix estimated from 10 ten-minute simulations of the spatial inflow turbulence field. The first nine eigenmodes ϕ_i are shown in Fig. 2 along with the fraction of energy in each mode. Note that these first nine eigenmodes resemble low-gradient functional shapes. We shall see later that more complex higher modes may not be needed to obtain accurate wind turbine response statistics. The eigenvalues, λ_i, of the sample covariance matrix (which describe the energy) of the first forty POD modes are shown in Fig. 3. The first few modes carry a significant portion of the energy of the entire turbulence field. Figure 4 shows power spectral density (PSD) function estimates of the orthogonal sub-processes $a_i(t)$ of the 1st, 2nd, 5th, and 100th modes. This illustrates how the energy of each sub-process varies with frequency – at low frequencies, PSD estimates associated with the first few eigenmodes are far more dominant than at higher frequencies where PSDs of all the sub-processes converge to the same level. This suggests that a few POD modes are adequate to capture the low-frequency characteristics of the inflow turbulence field but to obtain a correct representation of the high-frequency content, a larger number of modes may be required. More details related to the efficiency of POD in describing inflow turbulence fields have been discussed in an earlier work of the authors (Saranyasoontorn & Manuel, 2005).

3.2 *Influence of POD inflow modes on turbine load statistics*

Having estimated inflow POD modes, it is of interest next to assess how many and which of these modes are needed to accurately obtain turbine load statistics. Here, we seek to estimate the variance and ten-minute extremes of (i) the flapwise bending moment (FBM) at the root of a turbine blade, (ii) the edgewise bending moment (EBM) also at the blade root, and (iii) the fore-aft tower bending moment (TBM) at the base. (FBM is the bending moment about the chord line of the blade airfoil while EBM is the bending moment about an axis perpendicular to the pitch axis and the chord line. With zero pitch and twist, FBM and EBM are the out-of-plane and in-plane blade bending moments, respectively.) The wind turbine simulation software, FAST (Fatigue, Aerodynamics, Structures, and Turbulence) (Jonkman & Buhl, 2004), was employed for the turbine load calculations subjected to various inflow fields.

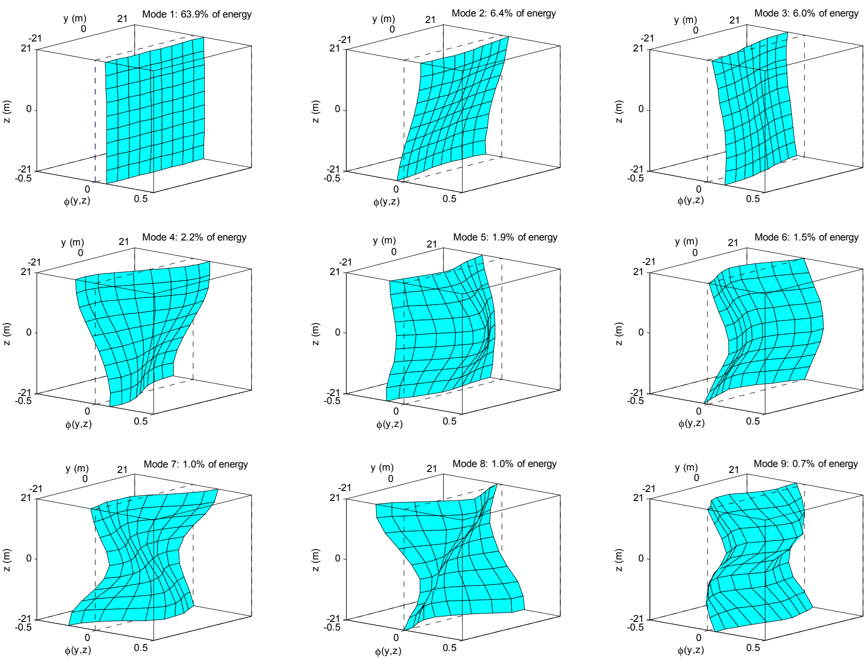

Figure 2. First 9 (out of 100) eigenmodes of the simulated along-wind turbulence field over the 42 m × 42 m rotor plane of the ART machine with the corresponding fraction of total energy .

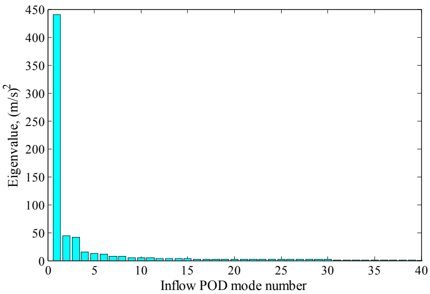

Figure 3. First 40 (out of 100) eigenvalues, λ_i, of the covariance matrix of the simulated along-wind turbulence field.

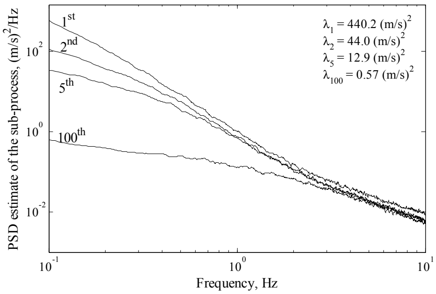

Figure 4. PSD estimates of the 1st, 2nd, 5th, and 100th orthogonal sub-processes a_i along with the corresponding energy, λ_i.

Figures 5, 6, and 7 show PSD estimates of the FBM, EBM, and TBM processes, respectively, derived based on 1, 5, 10, and 20 inflow POD modes compared with target spectra (based on full-field simulations, i.e., all 100 modes). Rotational sampling effects (i.e., sampling of the inflow turbulence by rotating blades of the turbine) are responsible for the presence of integer multiples of the rotational frequency (1P) of the turbine; this results in PSD peaks at 0.7 Hz (1P), 1.4 Hz (2P), 2.1 Hz (3P), etc. A resonance peak at the first TBM natural frequency (≈0.85 Hz) is also evident in both FBM and TBM spectra (Figs. 5 and 7). Overall, we see that a small number of inflow modes is sufficient to capture most of the power at low frequencies. As a result, low-dimensional POD representations of the inflow may be efficient for use in predicting second-order statistics of turbine loads that have large energy at low frequencies. Note that the dominant peak at 1P in the EBM spectra (in Fig. 6) results from gravity loading (i.e., due to the self weight of the blades), which explains why a single POD mode appears to capture virtually the entire energy content present at that at the rotational frequency. Note, too, that an important peak at 1P in the FBM spectra in Fig. 5 is well resolved since this peak is driven mainly by the vertical wind shear over the rotor plane and is thus insensitive to the inflow turbulence.

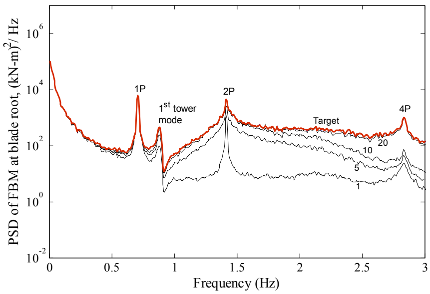

Figure 5. Contribution of 1, 5, 10, and 20 inflow POD modes to the PSD of the FBM at the blade root compared with the target PSD based on full-field inflow simulation.

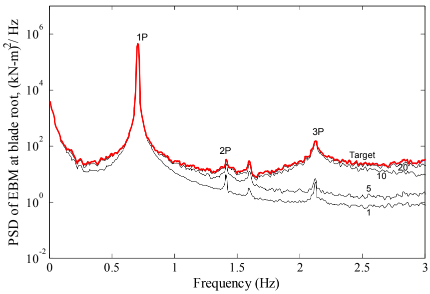

Figure 6. Contribution of 1, 5, 10, and 20 inflow POD modes to the PSD of the EBM at the blade root compared with the target PSD based on full-field inflow simulation.

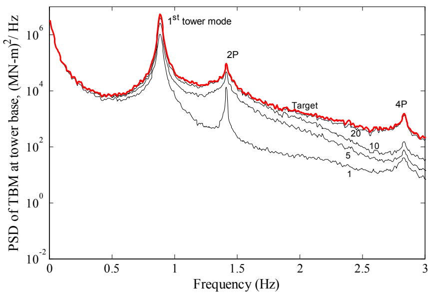

Figure 7. Contribution of 1, 5, 10, and 20 inflow POD modes to the PSD of the TBM at the base compared with the target PSD based on full-field inflow simulation.

Figure 8 shows the ratio of the POD-based variance (averaged over 10 ten-minute simulations) to the variance based on full-field simulation for each of the turbine load measures. The variance of the EBM process converges rapidly with increased number of POD modes due to the dominance of the gravitational loading. For FBM and TBM, a larger number of inflow POD modes is needed to achieve the same accuracy that is possible with a few modes for EBM. The variance of the FBM process approaches the full-field value faster than does the TBM because, for the FBM, a proportionately larger amount of energy is concentrated at 1P and lower frequencies (see Fig. 5) where a small number of POD modes can accurately describe the inflow turbulence field. Note that a peak at the rotational frequency (1P) in the TBM PSD is absent since at two instants in each turbine rotation, the TBM resulting from shear forces at the blade roots is the same; thus, for a two-bladed turbine, only 2P and higher even harmonics result.

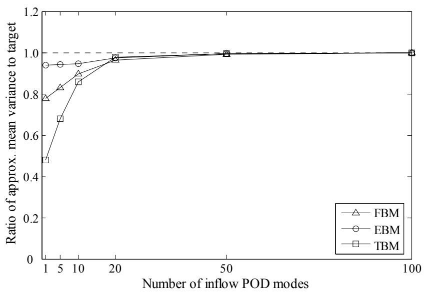

Figure 8. Ratio of variance of turbine load measures based on 1, 5, 10, 20, and 50 POD modes to that based on full-field inflow simulation.

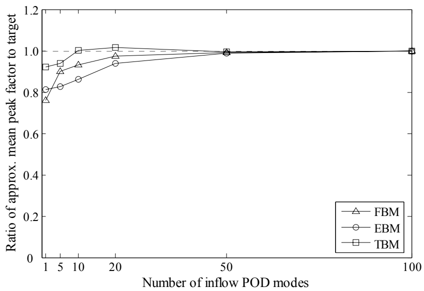

Figure 9. Ratio of ten-minute peak factor of turbine load measures based on 1, 5, 10, 20, and 50 POD modes to that based on full-field inflow simulation.

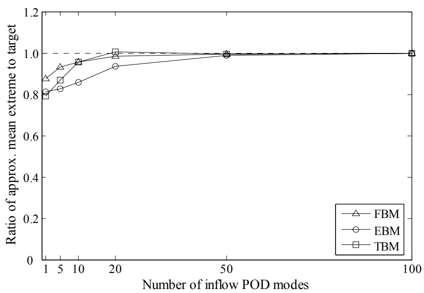

Figure 10. Ratio of mean ten-minute extreme turbine load measures based on 1, 5, 10, 20, and 50 POD modes to that based on full-field inflow simulation.

Convergence of the ten-minute peak factor and the mean ten-minute extreme of the load measures is illustrated in Figs. 9 and 10, respectively. Fast convergence rates are found for FBM and TBM. The slower rate of convergence for the ten-minute peak factor and extreme of the EBM is possibly due to the highly non-Gaussian (bimodal) characteristics of the EBM process which has significant probability mass due to gravity cycles as well as turbulence.

4 EFFECT OF INFLOW TURBULENCE SAMPLING ON LOADS

A POD analysis of an inflow turbulence field can be carried out at a site by employing a sample covariance matrix estimated from measured inflow data there. It is expected that a finer resolution in spatial and temporal scales of the inflow data should provide a better estimates of the POD modes and thus of turbine loads. It is well recognized that inflow instrumentation arrays at high elevations and over large spatial dimensions such as those needed for commercial wind turbine applications can be expensive. Hence, it may be worthwhile to assess what would be appropriate and efficient sampling resolutions of inflow data to accurately predict turbine loads. We can do this by first assessing how such data should be sampled to determine the important POD modes that drive these loads. Accordingly, next, we investigate (i) how spatially dense do we need to make our inflow spatial sensor arrays, and (ii) how fast a sampling rate do we need in order that a POD analysis can be performed which will lead to accurate wind turbine load predictions.

4.1 *Spatial sampling issues*

It was shown earlier that the first ten POD modes extracted from the inflow data simulated on a 10×10 grid are sufficient for use in predicting the wind turbine load statistics (FBM, EBM, and TBM variance and extremes, for example). This suggests that the low-gradient spatial patterns of the inflow turbulence field associated with the first modes (see Fig. 2) are most important in establishing loads. From a practical point of view, then, it may be unnecessary to collect inflow data at very fine spatial resolutions in order to estimate more complex POD modes. To investigate this issue, we carried out a sensitivity study of turbine load statistics to different spatial samplings of inflow data. This was done by employing different spatial grids or sensor arrays on the rotor plane of Fig. 1(b). Table 1 summarizes turbine load statistics derived based on 10 inflow POD modes obtained from data on 4×4, 6×6, 8×8, and 10×10 grids. Note that the load statistics are presented as ratios to those obtained using a full-field inflow description on a 10×10 grid. The full-field load statistics are included in the bottom row of Table 1.

Table 1. Turbine load statistics using 10 inflow POD modes derived from different spatial grid arrangements (expressed as a ratio to statistics derived from full-field simulation on a 10×10 grid). The actual values of the statistics for the full-field simulation are shown in bold face in the last row of the table.

Grid	Variance			10-minute Peak factor			Mean 10-minute Extreme		
	FBM	EBM	TBM	FBM	EBM	TBM	FBM	EBM	TBM
4×4	0.87	0.95	0.92	0.92	0.88	0.98	0.95	0.87	0.97
6×6	0.87	0.95	0.84	0.92	0.87	1.01	0.95	0.87	0.96
8×8	0.85	0.95	0.80	0.95	0.88	0.98	0.95	0.87	0.93
10×10	0.90	0.95	0.86	0.93	0.86	1.00	0.96	0.86	0.95
10×10 (full-field)	**4.45×10^3 $(kN\text{-}m)^2$**	**8.03×10^3 $(kN\text{-}m)^2$**	**3.19×10^5 $(kN\text{-}m)^2$**	**3.16**	**2.26**	**3.39**	**5.44×10^2 (kN-m)**	**2.30×10^2 (kN-m)**	**3.32×10^3 (kN-m)**

Note that the load predictions in Table 1 have two sources of error: (i) due to truncation at the 10th POD mode; and (ii) due to the spatial interpolation of aerodynamic forces in the turbine response simulations. It is seen in Table 1 that load statistics of the EBM process are almost independent of the spatial resolution of the inflow data. This is again because EBM is driven mainly by gravity loading from the self weight of the blades, not by inflow turbulence. This is verified in Fig. 11 which shows the effect of turbulence on PSD estimates of EBM. Clearly, the dominant PSD peak at the rotational frequency of 0.7 Hz (1P) is well represented in both cases, leading to a small difference in the variance for the two cases (as is indicated on the plots in Fig. 11).

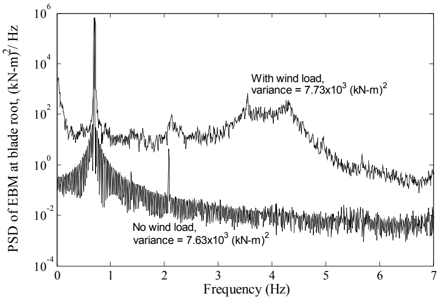

Figure 11. Comparison of the estimates of the EBM process showing influence of aerodynamic forces.

Variance estimates of FBM and TBM are seen to depend on the resolution of the sampling sensor array but variations are small and unsystematic. Any large errors that result from interpolation of aerodynamic forces on a coarse grid are offset by the fact that on a coarse grid, 10 POD modes retain a greater percent of the overall energy in the inflow turbulence field. The ten-minute peak factors and extremes of these two turbine loads (FBM and TBM) are rather insensitive to the sensor distribution. This is because the important low-gradient eigenmodes that most influence turbine load statistics can be extracted reasonably well by employing a small number of inflow data streams. In other words, the use of inflow sensor arrays with very fine spatial resolution may be unnecessary for establishing wind turbine loads. For this particular case, sampling of the inflow data on a sparse 4×4 grid, corresponding to a spatial resolution of about one-third the rotor diameter, can lead to reasonable accuracy in wind turbine load predictions.

4.2 *Temporal sampling issues*

In the interest of economy again, it is useful to study the influence of different temporal sampling rates for the inflow data on turbine load statistics predicted based on a POD analysis. Such a study amounts essentially to assessing the importance of low and high frequencies in the various turbine loads. We saw earlier that a 4×4 spatial grid (at a 20 Hz sampling rate) was adequate for obtaining the first 10 POD modes and led to fairly accurate load statistics. Accordingly, now we investigate estimates of turbine load statistics based on 10 POD modes derived from inflow data simulated on the same 4×4 grid but with slower sampling rates of 1.25, 2.5, 5, 10, and 20 Hz. The resulting load statistics are then compared with those derived based on full-field inflow simulation on a 10×10 grid where a sampling rate of 20 Hz was used. Results are tabulated in Table 2.

Table 2. Turbine load statistics using 10 inflow POD modes derived from inflow data measured on a 4×4 grid at different sampling rates (expressed as a ratio to statistics derived from full-field simulation on a 10×10 grid with a rate of 20 Hz – see Table 1).

Sampling rate (Hz)	Variance			10-minute Peak factor			Mean 10-minute Extreme		
	FBM	EBM	TBM	FBM	EBM	TBM	FBM	EBM	TBM
1.25	0.83	0.94	0.55	0.90	0.83	0.94	0.94	0.83	0.83
2.5	0.85	0.95	0.81	0.91	0.85	1.01	0.94	0.85	0.95
5.0	0.86	0.95	0.86	0.90	0.85	0.99	0.94	0.85	0.95
10.0	0.87	0.95	0.91	0.92	0.87	0.99	0.95	0.86	0.97
20.0	0.87	0.95	0.92	0.92	0.88	0.98	0.95	0.87	0.97

The variance of the EBM process is seen to not be sensitive to the sampling rate of the inflow turbulence data as should be expected. This can be confirmed from Fig. 11 where it is clear that inflow turbulence (and thus its sampling rate) are not important; only gravity loads matter.

In the case of the FBM and TBM processes, it is worthwhile to study PSDs for different sampling rates as is done for the two cases in Figs. 12 and 13, respectively, where estimates from sampling rates of 1.25 and 20 Hz are compared. It is seen that the energy content at low frequencies can be resolved almost perfectly regardless of sampling rate. In the case of FBM, most of the energy is concentrated in such frequency regions (at and below 1P) leading to small changes in variance estimates as lower sampling rates are employed to collect the inflow data. In contrast, for the TBM process, with the slowest sampling rate of 1.25 Hz, the resonant peak of the first tower bending natural mode at around 0.85 Hz cannot be recovered satisfactorily. This explains why the accuracy of the variance estimates of the TBM decreases noticeably at this low sampling rate of 1.25 Hz.

The ten-minute peak factor estimates are not very sensitive to the sampling rate for all the load measures. Both variance and peak factors influence ten-minute extreme values; hence, TBM extremes are somewhat affected by the sampling rate.

These various results suggest that, at least in this particular case, inflow turbulence data may be sampled at a fairly slow rate (even as slow as 1.25 Hz) without introducing significant error in estimates of turbine blade load statistics. However, somewhat faster rates (greater than 2.5-5 Hz) may be required to achieve accuracy in tower bending loads.

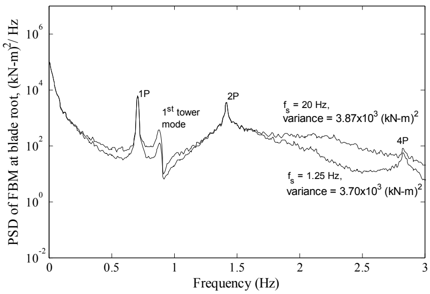

Figure 12. PSD estimates of the FBM at the blade root based on 10 inflow POD modes extracted from inflow simulated on a 4×4 grid at sampling frequencies, f_s, of 20 Hz and 1.25 Hz.

5 CONCLUSIONS

The application of Proper Orthogonal Decomposition (POD) techniques has been presented for characterization of the inflow turbulence random field experienced by a wind turbine. We have evaluated the efficiency of reduced-order POD models of the inflow turbulence field for use in predicting wind turbine loads.

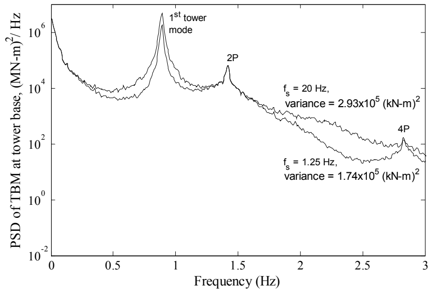

Figure 13. PSD estimates of the TBM at the base based on 10 inflow POD modes extracted from inflow simulated on a 4×4 grid at sampling frequencies, f_s, of 20 Hz and 1.25 Hz.

Numerical examples presented involved POD analysis of along-wind turbulence data simulated for a 10×10 square grid discretization over the rotor plane of a typical two-bladed wind turbine based on the Kaimal spectral model and an exponential coherence model. In general, a small number of POD modes could efficiently and accurately account for the low-frequency energy in the turbine load measures studied. At high frequencies, a larger number of modes was required. The appropriate number of inflow POD modes needed to adequately describe each load type also depends on the dynamical characteristics of that load. Integer multiples of the rotational frequency (1P) of the turbine due to sampling of the inflow turbulence by rotating blades of the turbine directly affect blade loads and the ability to describe these harmonic modes affects the accuracy of blade load statistics for any POD representation. For the fore-aft tower bending loads, the 1P peak is absent; therefore, accurate loads can be derived from a limited number of inflow POD modes only if the resonant peak at the first tower natural frequency could be recovered.

Sensitivity of load statistics to different spatial and temporal sampling resolutions of the inflow turbulence data was investigated. With respect to spatial resolution, it was found that spatial sampling of inflow turbulence data on a sparse 4×4 grid, corresponding to a spatial resolution of about one-third the rotor diameter, can lead to reasonable accuracy in predictions of wind turbine blade and tower loads. With respect to temporal sampling, it was found that, for the particular turbine studied, inflow turbulence data could be sampled at a fairly slow rate (even as slow as 1.25 Hz) without introducing significant error in estimates of turbine blade load statistics. However, somewhat faster rates (greater than 2.5-5 Hz) are required to achieve similar accuracy in tower bending loads.

While the various results obtained were based on a single turbulence spectral and coherence model and apply to a specific wind turbine, useful insights can be gained from a POD analysis such as are discussed above. The influence of the spectral character and coherence structure of the inflow turbulence random field, the rotor aerodynamics, and the structural dynamics of the turbine all have influence on the accuracy of any low-dimensional POD-based turbine load prediction. Moreover, a given POD representation can lead to varying accuracy for different turbine load types. Similar POD-based studies on other turbines and for different inflow models can advance our understanding of the characteristics of inflow turbulence that most influence various wind turbine loads.

ACKNOWLEDGEMENTS

The authors gratefully acknowledge the financial support provided by Grant No. 30914 from Sandia National Laboratories. They also thank Drs. Alan Wright and Maureen Hand of the National Renewable Energy Laboratory (NREL) for providing us with the wind turbine model used for the simulations.

REFERENCES

Buhl, M.L. Jr. 2003. *SNwind User's Guide*, National Renewable Energy Laboratory, Colorado.

Carassale, L. & Solari, G. 2000. Proper Orthogonal Decomposition of Multi-Variate Loading Processes. *Proc. 8th ASCE Joint Specialty Conference on Probabilistic Mechanics and Structural Reliability*, Indiana.

Chen, X. & Kareem, A. 2003. POD in reduced order modeling of dynamic load effects, *Proc. 9th International Conference on Applications of Statistics and Probability in Civil Engineering*. Vol. 2, California, pp. 1591-1598.

Holmes, P.J., Lumley J.L. & Berkooz, G. 1996. *Turbulence, Coherent Structures, Dynamical Systems and Symmetry.* Cambridge Monogr. Mech., Cambridge University Press.

Holmes, P.J., Lumley, J.L., Berkooz, G., Mattingly, J.C. & Wittenberg, R.W. 1997. Low-Dimensional Models of Coherent Structures in Turbulence. *Physics Reports*, Vol. 287: 337-384.

IEC. 1998. *Wind Turbine Generator Systems Part 1: Safety Requirements*. International Electrotechnical Commission (IEC), IEC/TC 88 61400-1, 2nd Ed., Geneva.

Karhunen, K. 1946. Zur Spektraltheorie stochastischer Prozesse. *Ann. Acad. Sci. Fennicae*, pp. 34.

Kosambi, D.D. 1943. Statistics in function space. *J. of Indian Math. Soc.*, Vol. 7: 76–88.

Jonkman, J.M. & Buhl, M.L. Jr. 2004. *FAST User's Guide*. Report No. NREL/EL-500-29798, National Renewable Energy Laboratory, Colorado.

Loève, M. 1948. Fonctions aléatoires du second ordre. In P. Lévy, Editor, *Processus stochastiques et mouvement Brownien*, Guathier – Villars, Paris, pp. 299.

Lumley, J.L. 1970. *Stochastic Tools in Turbulence*. Academic Press, New York.

Saranyasoontorn, K. & Manuel, L. 2005. Low-Dimensional Representations of Wind Turbine Inflow Turbulence and Response using Proper Orthogonal Decomposition. *Proc. of the ASME Wind Energy Symposium*, AIAA, Nevada, pp. 541-551.

Spitler, J.E., Morton, S.A., Naughton, J.W. & Lindberg, W.R. 2004. Initial Studies of Low-Order Turbulence Modeling of the Wind Turbine In-flow Environment. *Proc. of the ASME Wind Energy Symposium*, AIAA, Nevada, pp. 442-451.